PHILOSOPHICAL TRANSACTIONS OF THE ROYAL SOCIETY A MATHEMATICAL, PHYSICAL & ENGINEERING SCIENCES

The Velocity Structure of the Upper Ocean in the Presence of Surface Forcing and Mesoscale Oceanic Eddies

R. A. Weller and D. Halpern

Phil. Trans. R. Soc. Lond. A 1983 **308**, 327-340
doi: 10.1098/rsta.1983.0007

Phil. Trans. R. Soc. Lond. A **308**, 327–340 (1983)
Printed in Great Britain

The velocity structure of the upper ocean in the presence of surface forcing and mesoscale oceanic eddies

By R. A. Weller† and D. Halpern‡

† *Woods Hole Oceanographic Institution, Woods Hole, Massachusetts* 02543, *U.S.A.*
‡ *NOAA Pacific Marine Environmental Laboratory, Seattle, Washington* 98105, *U.S.A.*

One goal of the Joint Air–Sea Interaction Experiment (JASIN) was to investigate the structure of the near-surface velocity field and to attempt to quantify what fraction of that field was related to the local wind. Toward that end, in the late summer of 1978, two moorings were deployed in the northern Rockall Trough with oceanographic instrumentation concentrated in the upper 100 m of the ocean. Simultaneous observations were made of the surface winds at each mooring and, adjacent to one of the moorings, of the velocity field at depths from 79 to 1000 m. Energetic, eddy-like circulation dominated the velocity field in the JASIN area at depths shallower than approximately 800 m. However, both the velocity and the vertical shear of horizontal velocity showed variability that increased with proximity to the surface.

Empirical orthogonal functions, computed to separate the velocity data into uncorrelated modes of variability, showed that over 97 % of the variability in the upper 300 m was distributed among only three vertical modes. The first function had little depth dependence; the second had strong depth-independent flow in the depth range of the mixed layer and weak flow in the opposite direction at all depths below; and the third had strong flow near the surface, strong flow in the opposite direction just below the base of the mixed layer, and weaker flow at all other depths. Function 1 alone provided a near-complete description of the velocity variability below 85 m, where the flows associated with the eddy-like circulation and the barotropic semidiurnal tide were the dominant components. At 85 m and above all three functions were necessary to provide a complete description. Temporal variability of function 2 was coherent with the local wind stress at the inertial frequency, but, at lower frequencies, resulted in transport in the mixed layer to the southeast that was not coherent with the local wind. Low frequency temporal variability of function 3 was coherent with the local wind stress; at these frequencies the velocity vector of function 3 nearest the surface was directed to the right of the wind stress vector and the velocity vector just below the base of the mixed layer was directed to the left of the wind stress. Thus, forcing by the local wind can account for some but not all of the increased variability found near the surface.

1. Introduction

This paper uses data from three JASIN oceanographic moorings to describe the variability and structure of the horizontal velocity field in the upper 300 m, and to examine the relation of that variability and structure to the forcing present at the sea surface, the local wind stress. Of particular interest were the following questions. (i) What fraction of the variability in the upper ocean was related to the local wind? (ii) Could horizontal variations in near-surface currents be related to horizontal variations in the wind field? (iii) Can the observed advection of properties in the mixed layer be attributed to the observed quasigeostrophic flow plus an Ekman velocity predicted from the observed wind stress?

Details of the moorings and instrumentation and an overview of pertinent meteorological and oceanographic data are given in §2. Section 3 discusses the structure and variability of the

velocity field, and §4, its relation to the local wind stress. A brief summary and discussion is given in §5.

2. Instrumentation and an overview of meteorological and oceanographic conditions during JASIN 1978

(*a*) *Instrumentation*

Three moorings, W1, W2, and H2, located at two sites 44 km apart provided the velocity data. W1 (12° 32′ W, 59° 01′ N) and W2 (12° 33′ W, 59° 01.5′ N) were located in the Fixed Intensive Array (FIA) of oceanographic moorings, and H2 (12° 30′ W, 59° 25′ N) was located at the northern boundary of the Oceanographic Intensive Area (OIA). H2 was in place from 16 July to 3 September 1978 and was a surface mooring with current meters concentrated between 60 m and the surface. W1 and W2 were in place from 30 July to 7 September 1978. W2 was a surface mooring with current meters concentrated between 85 m and the surface. W1 was a subsurface mooring located 1.2 km southeast of W2 with current meters between 79 and 1000 m. H2 had seven current meters, mostly vector-averaging current meters (VACMs, manufactured by EG&G Sea-Link). W2 had eight vector-measuring current meters (VMCMs, Weller & Davis 1980) and one VACM. W1 had 23 VACMs. The moorings and the performance of the current meters have been discussed elsewhere (Halpern *et al.* 1981).

(*b*) *Meteorological conditions*

The H2 surface buoy had a vector-measuring wind recorder (VMWR, adapted from a VMCM) that used orthogonal propeller sensors to measure the wind velocity 3.5 m above the sea surface. The W2 surface buoy had a VMWR and a vector-averaging wind recorder (VAWR, Payne 1974), both mounted at 3.5 m. Wind stress was calculated from the records by using Large & Pond's (1982) speed-dependent formulation for the drag coefficient, after logarithmic extrapolation to 10 m. The wind records from the two sites were highly coherent; the wind stress over the JASIN area had little spatial variability (see Guymer *et al.* this symposium, as well as Weller *et al.* (1980)) and did not during this experiment provide a direct source of horizontal variability in the near-surface currents (figure 1).

(*c*) *Oceanographic conditions*

The depth of the mixed layer shoaled from 15 m to within several metres of the surface at the end of July and in early August when the wind speed dropped to below 5 m s^{-1}. Similar events happened on 25–27 August and on 2–3 September. The mixed layer deepened between 1 and 25 August to a maximum depth of 35 m in response to several strong wind events.

The mesoscale circulation (see Ellett *et al.* this symposium; Pollard 1982) was dominated by energetic eddies that moved northwestward at *ca.* 2 cm s^{-1} (Van Aken & Prangsma 1981) through the array of moorings. Veering of the flow from northward to southward as the eddy field moved occurred on 4–5 August at H2 and on 19 August at W2 (figure 2).

3. The horizontal velocities observed at H2 and at W1 and W2

The current meter data from W1 and W2, taken together, provide a good description of the vertical structure of the velocity at one location. The H2 current meter data provide a contrasting view of the flow in the upper 100 m at a site removed from W2 by a distance of 44 km. At W1

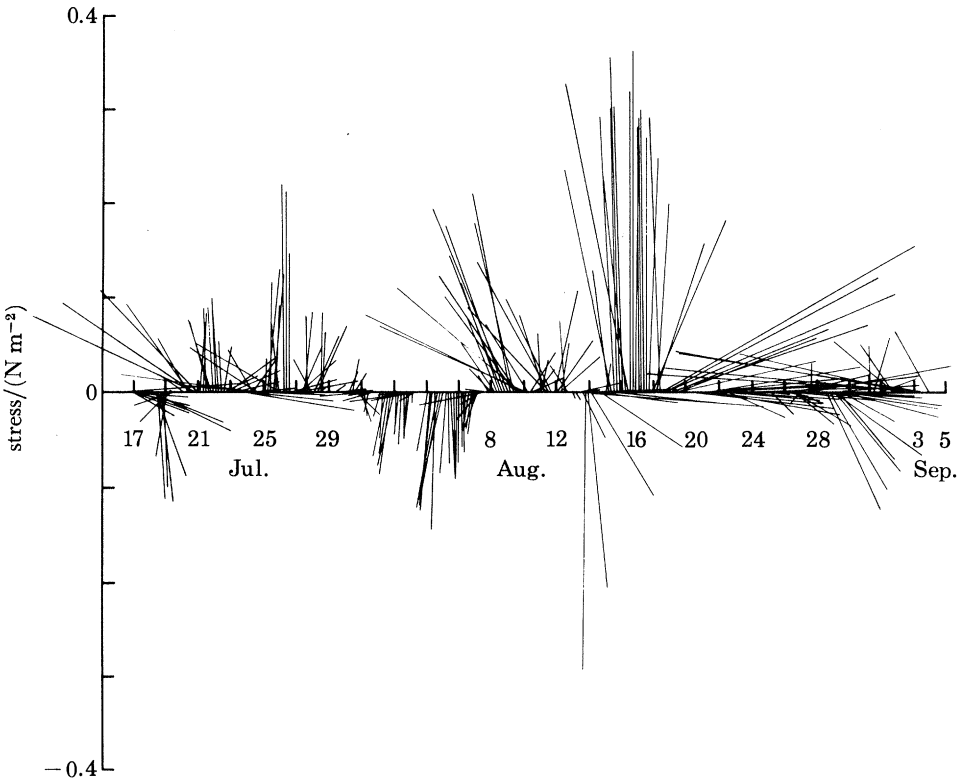

FIGURE 1. The wind stress record during JASIN 1978, compiled by merging wind stress records from the instruments on H2 and W2. Plots are of hourly averaged stress vectors; flow to the north is up and flow to the east is to the right.

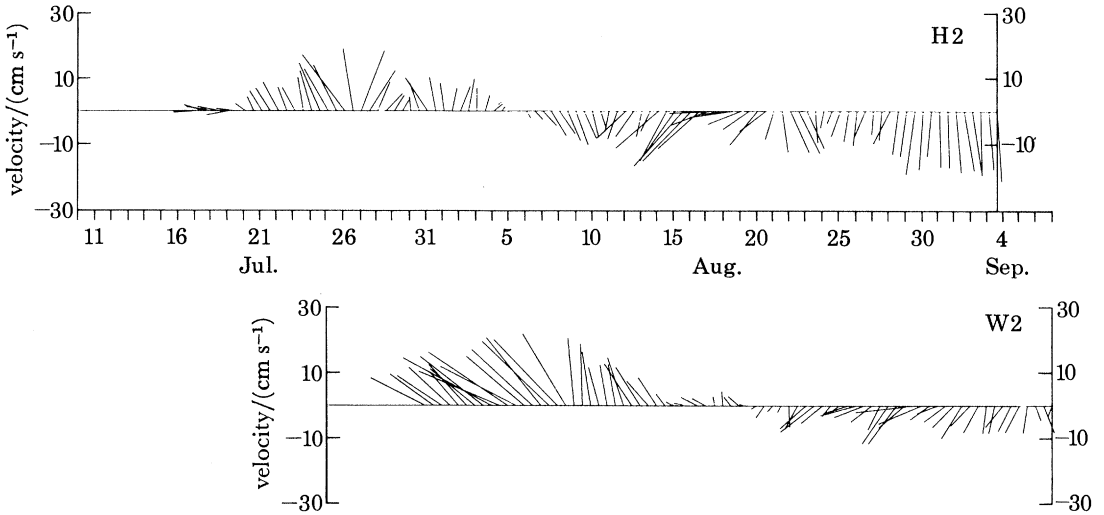

FIGURE 2. Flow at H2 (at 60 m) and at W2 (at 85 m). Plots are of 12.5 h average velocity vectors; flow to the north is up and flow to the east is to the right.

there was little variation with depth of the flow between 79 and 300 m. A depth of 1000 m was below the depth of penetration of the eddies and the flow there had a smaller magnitude, especially before 13 August. At W2 the flow at the deeper instruments was virtually identical to the flow at the shallow instruments on W1, but that similarity decreased with proximity to the surface. The flow at H2 was, like the flow at W1 and W2, dominated by the eddy circulation; and, like the flow at W2, the flow at H2 nearest the surface (3 m) was most different from the deepest (60 m) flow.

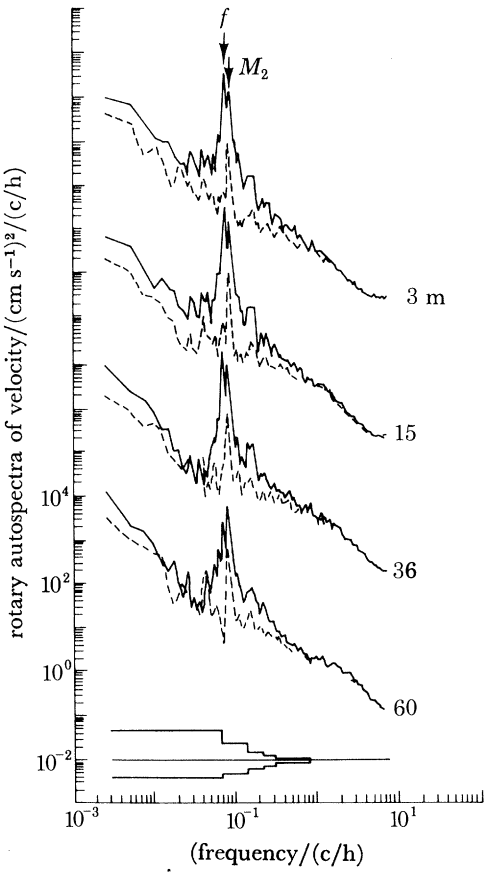

FIGURE 3. Rotary autospectra of horizontal velocity at 3, 15, 36 and 60 m at H2. Confidence limits (95%) are shown below the spectra. The solid lines are the clockwise ($\omega < 0$) spectra, and the dashed lines are the counterclockwise ($\omega > 0$) spectra. The 3, 15 and 36 m spectra are plotted three decades above the spectrum from the next deepest record.

Rotary autospectra were computed to examine the distribution of velocity variability over a range of frequencies both positive, corresponding to velocity vectors that rotate counterclockwise with time, and negative, corresponding to a velocity vector that rotates clockwise with time. Rotary autospectra of four full-length velocity records from H2 (3, 15, 36, and 60 m, figure 3) show a depth dependence typical of either mooring site. Two peaks, near 0.07 and 0.08 c/h, dominate the spectra, but their relative magnitudes change as a function of depth. The peak near 0.07 c/h in the clockwise spectra is associated with oscillatory flow at the inertial period ($12/\sin\phi$ hours, where ϕ is the latitude). The inertial motion is depth-independent in the mixed layer and an order of magnitude smaller in amplitude below the mixed layer (Weller

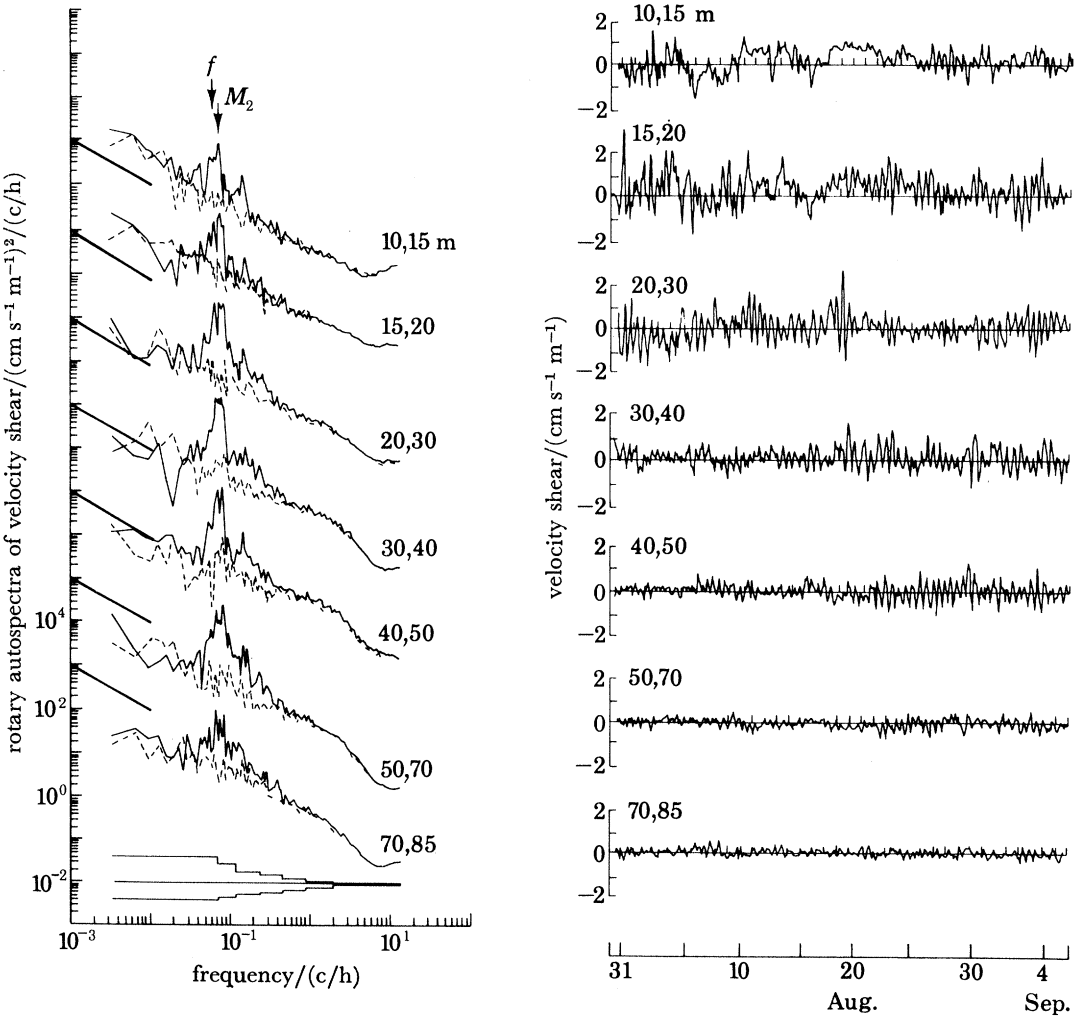

FIGURE 4. Time series of the vertical shear of horizontal velocity calculated from current meter records from W2 (right). The pair of numbers, 10, 15, for example, indicates the depths (in metres) of the two current meter records used to calculate the shear. Rotary autospectra of vertical shear of horizontal velocity (left). Each spectrum is plotted two decades above the spectrum from the next deepest record. Confidence limits (95%) are drawn below the spectra. Lines with slope of -1 are drawn between 10^{-3} and 10^{-2} c/h and are spaced two decades apart. The deeper, less energetic spectra fall beneath these reference lines.

1982). The peak near 0.08 c/h is associated with the semidiurnal tidal components (M_2, at 0.0805 c/h, S_2, at 0.0833 c/h, and N_2, at 0.0790 c/h) of the flow; the tidal flow was elliptical, with spectral peaks in both the clockwise and counterclockwise spectra, and changed little in magnitude or direction with depth. Smaller spectral peaks show at frequencies $M_2 + f$ and $2M_2$. The spectra have high frequency shoulders or breaks in slope in the range 1–4 c/h. Near the surface at low frequencies and at all depths near the inertial frequency the clockwise rotating velocity components were more energetic than the counterclockwise components at the same frequencies.

Time series of the vertical shear of the horizontal velocity (figure 4), calculated by subtracting the velocity record at one depth from that just above it and then dividing the result by the depth separating the two current meters, show that shear in the mixed layer was larger than that below the mixed layer. Between 10 and 15 m, for a period of days, 17–25 August, mean shear of 10^{-2} s^{-1}

persists; rotary autospectra (figure 4) show that near the surface this low frequency component was the most energetic component of the shear. Across the base of the mixed layer the shear was dominated by a clockwise component in a frequency band around the inertial frequency. Below the mixed layer, the variability of the shear was reduced. The spectral levels of shear between 70 and 85 m, for example, were at all frequencies at least one order of magnitude lower than those between 10 and 15 m.

To examine further the distribution of velocity variability between various spatial scales in the upper ocean, empirical orthogonal functions were computed. Their computation and interpretation have been described by Davis (1976) and others. Briefly, the eigenvalues and eigenvectors of the covariance matrix of the velocity data are found. The eigenvectors of the covariance matrix are depth-dependent empirical functions that are uncorrelated modes of variability. The corresponding eigenvalue shows what fraction of the total velocity variance is associated with the function. The time-dependent amplitude of each eigenvector can be calculated; and, at a given depth, the contribution of one function to the velocity time series is the vector product of the amplitude time series and the vector at that depth from that function.

TABLE 1. EIGENVALUES OF THE W_2, W_1 (LEFT) AND H_2 (RIGHT) VELOCITY DATA

	eigenvalue $(\text{cm s}^{-1})^2$	percentage of the variance	cumulative percentage	eigenvalue $(\text{cm s}^{-1})^2$	percentage of the variance	cumulative percentage
(1)	0.751×10^4	87.02	87.02	0.598×10^4	87.17	87.17
(2)	0.755×10^3	8.75	95.77	0.779×10^3	11.36	98.53
(3)	0.126×10^3	1.46	97.23	0.673×10^2	0.98	99.51
(4)	0.734×10^2	0.85	98.08	0.330×10^2	0.48	99.99
(5)	0.495×10^2	0.57	98.65	0.686×10^1	0.01	100.00
(6)	0.299×10^2	0.35	99.00			
(7)	0.204×10^2	0.24	99.24			
	remaining eigenvalues	0.16	100.00			

At W2, W1 a vertical array was constructed from the W2 records taken together with the records from the W1 current meters at and between 88 and 310 m. Table 1 shows the distribution of variance among the eigenvalues for the W2, W1 data and among the eigenvalues of the H2 velocity data, computed from the five time series (3, 15, 19, 36 and 60 m) that ran the full length of the experiment.

The first three eigenvectors for W2, W1 and for H2 (figure 5) show that in each case the dominant eigenfunction has flow in similar direction and of similar magnitude at all depths. (The 79 m data was from a VACM, that at adjacent depths was from VMCMS. The vector at 79 m on W2, W1 is larger in magnitude than adjacent vectors, an indication of the over-response of a VACM on a surface mooring.) The second eigenvector has energetic flow with similar magnitude and direction at 20 m and above; below 20 m the flow decreases in magnitude and, at W2, W1, veers so that at depth it is antiparallel to the near-surface flow. The third eigenvector at each site shows surface flow with an antiparallel flow of similar magnitude just below; at depth at W2, W1 this eigenvector decays and veers. It is not certain that unique physical significance can be associated with each function, but because the functions are orthogonal the technique provides a method of separating for further analysis independent modes of variability, each associated with a different vertical function. Rotary autospectra of the temporal variability associated with each function at 10 m on W2 (figure 6) show the distribution in frequency of the variability. The first function has energetic tidal, but not inertial, variability and a nearly equal partition between

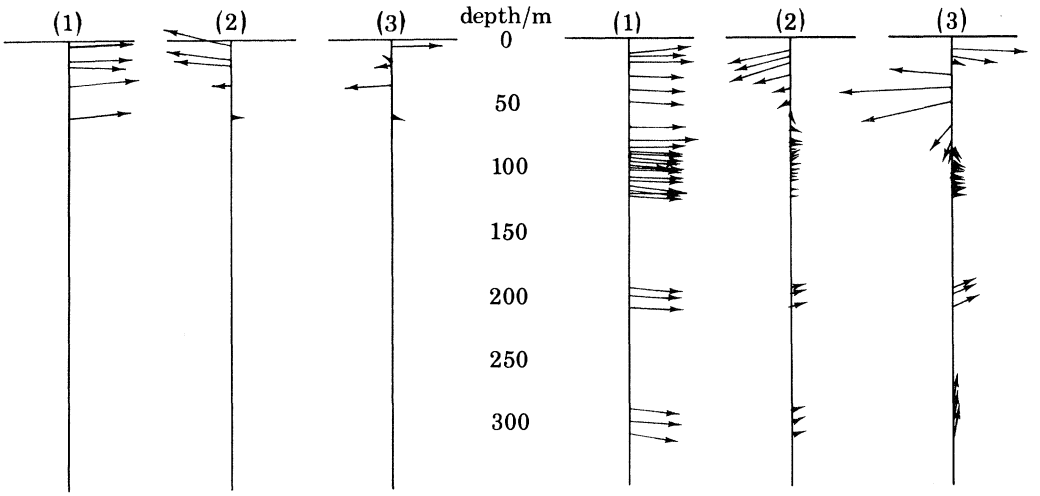

FIGURE 5. The first three eigenvectors for H2 (left) and for W2, W1 (right). At each depth the arrow represents a horizontal velocity vector. The figure is drawn to represent three dimensions. In the plane of the paper the z-axis is vertical and the x-axis is horizontal. The y-axis would be perpendicular to the z, x-plane. The viewer is looking down from 30° above the x, y-plane.

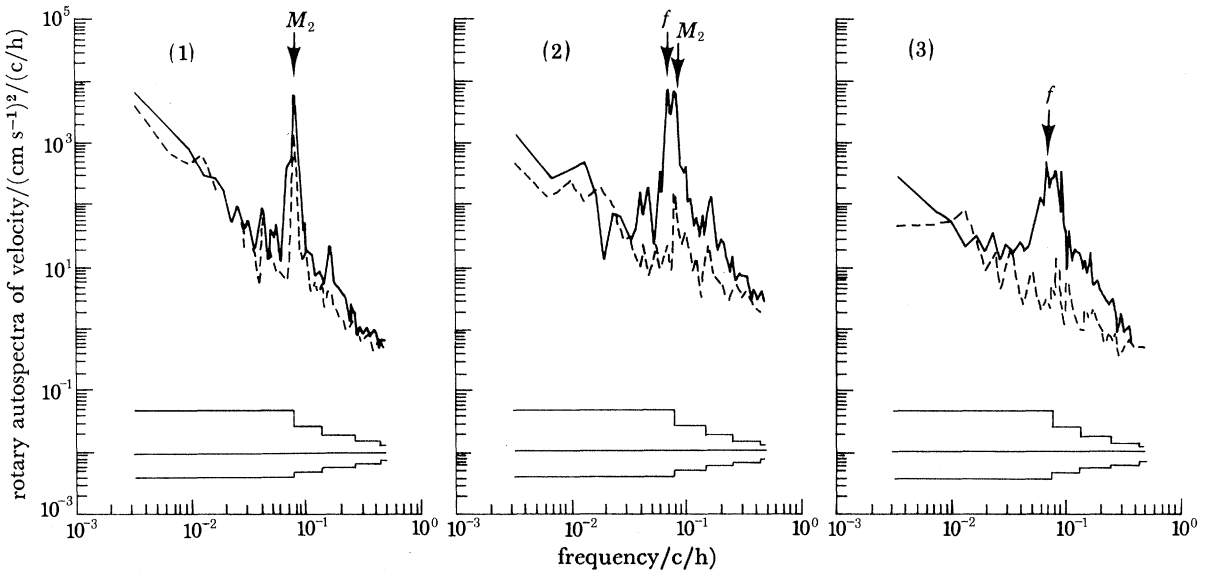

FIGURE 6. Rotary autospectra of the temporal variability of the dominant empirical orthogonal functions at W2. The time series are from 10 m at W2; 95% confidence limits are shown. The solid lines are the clockwise spectra, and the dashed lines are the counterclockwise spectra.

clockwise and counterclockwise components at inertial and tidal frequencies. Function 3 at W2, W1 shows, over a broad frequency band, greater variability in the clockwise rotary components. The progressive vector diagrams (figure 7) of these functions show the contribution each made to the flow at 10 m at W2. Only at depths shallower than 85 m does either function 2 or 3 contain more than 2% of the variability; below 85 m the variability of the flow is well represented by function 1 alone, which contains at least 93% of the variability. Above 85 m, however, modes of variability with smaller vertical scales (functions 2 and 3) contain as much as 34% and 11% of the variability, respectively.

PHILOSOPHICAL TRANSACTIONS OF THE ROYAL SOCIETY A MATHEMATICAL, PHYSICAL & ENGINEERING SCIENCES

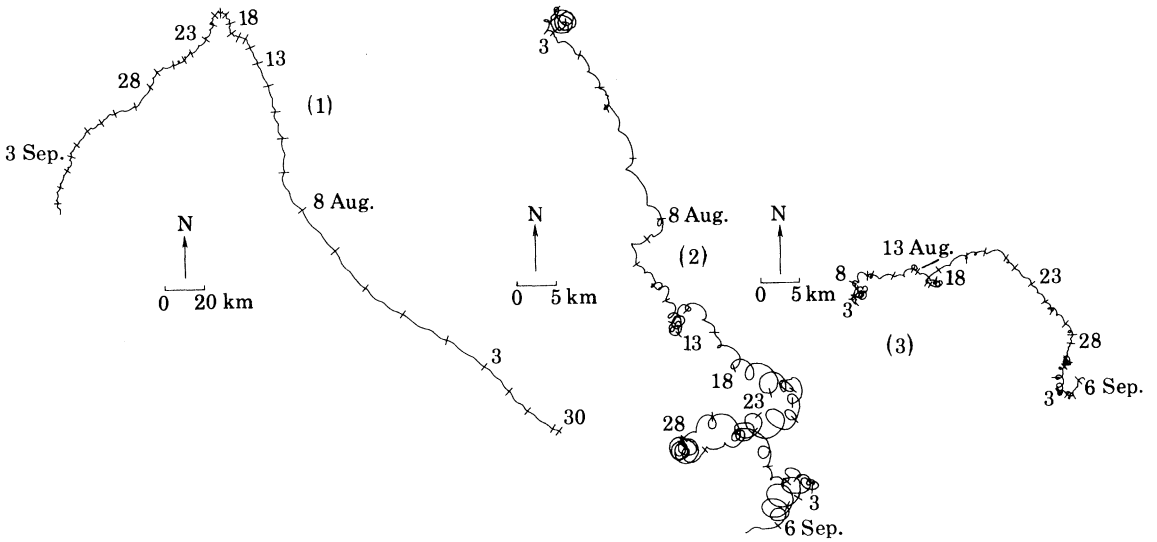

FIGURE 7. Progressive vector diagrams of the dominant functions at W2 (10 m). Ticks are located at 00h00 (G.M.T.) of each day, and the diagrams run from 20h00 on 30 July to 06h00 on 6 September. Note that the scales on the plots of functions 2 and 3 are smaller than that on the plot of function 1.

4. THE RELATION OF THE NEAR-SURFACE VARIABILITY TO THE WIND

While the flow associated with the quasigeostrophic eddy field dominated the low frequencies during JASIN 1978, there was, as shown by the magnitude of the eigenvalues of empirical orthogonal functions 2 and 3, increased velocity and shear variability unique to the near-surface. A fraction of that velocity variability near the surface was thought to be related to the local wind stress. Coherence (figure 8*a*) between the wind and the flow in the upper 70 m was found primarily at sub-inertial frequencies; flow in the upper 20 m that was coherent to the local wind was approximately 90° to the right of the wind while flow between 30 and 70 m that was coherent to the local wind was approximately 90° to the left. Coherence between the wind and flow below 70 m was found in narrow frequency bands near ± 0.02 and ± 0.09 c/h. A greater fraction of the variability in the velocity shear near the surface than in the velocity was related to the local wind stress (figure 8*b*).

In an attempt to isolate the variability unique to the near-surface region and to examine the structure of the response to the wind, the deepest velocity record available at H2, 60 m, and the deepest at W2, 85 m, were subtracted from the shallower records at H2 and W2, respectively. The deep records were from below the base of the mixed layer and, presumably, from below the region of direct frictional influence by the wind. The residual records, if wind-driven, should be similar at H2 and W2 because the wind stress at the two sites was highly coherent. Progressive vector diagrams show such similarity only between 15 and 25 August. In that period the near-surface flow was consistently to the right of the wind stress, veered further to the right with depth, and decayed with depth (figure 9). In that period, then, the near-surface flow resembled the flow predicted by the Ekman equations,

$$\frac{\partial u}{\partial t} - fv = \nu \frac{\partial^2 u}{\partial z^2}, \quad \frac{\partial v}{\partial t} + fu = \nu \frac{\partial^2 v}{\partial z^2},$$

where $\nu\rho\,\partial u/\partial z = \tau_x$ and $\nu\rho\,\partial v/\partial z = \tau_y$ at $z = 0$ and u and v go to zero as z goes to $-\infty$; τ_x and τ_y are the east and north components of the observed wind stress. Closest agreement between the

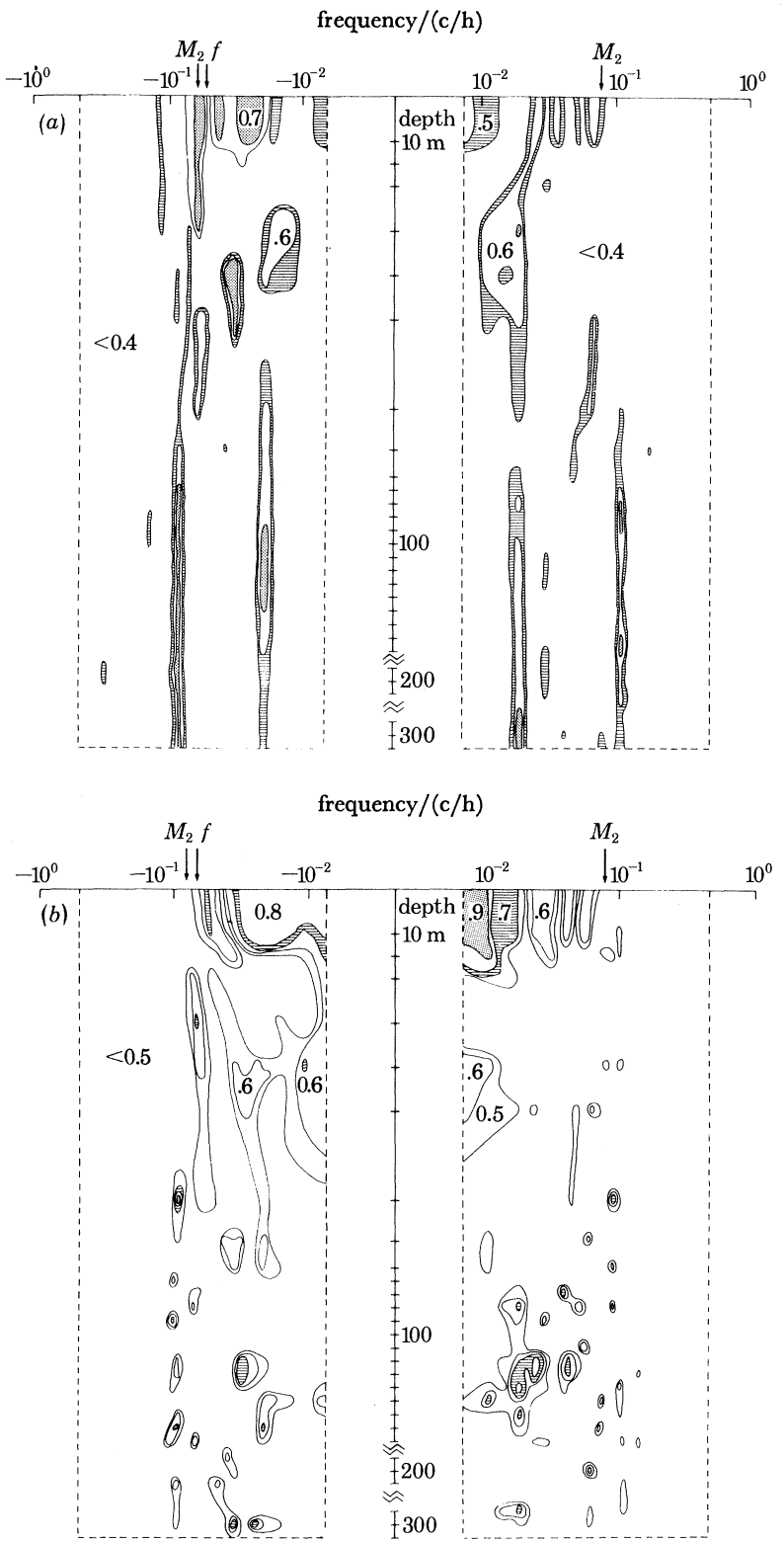

FIGURE 8. Contour diagrams of coherence between (*a*) the wind stress and the horizontal velocities at the depths of the instruments on W2 and W1 and (*b*) the wind stress and the vertical shear of horizontal velocity. The contour interval is 0.1. The 95% confidence level varied with frequency as shown in figure 10; the highest value of that level is 0.437.

PHILOSOPHICAL TRANSACTIONS OF THE ROYAL SOCIETY A MATHEMATICAL, PHYSICAL & ENGINEERING SCIENCES

flow observed at 10 m at W2 and the predicted flow was found with $\nu \approx 10^3\,\mathrm{cm^2\,s^{-1}}$. Much of the time, however, the residual flows near the surface at H2 and at W2 did not resemble each other or the predicted wind-driven flow. The residual flow retained a component that was different at H2 from that at W2 and that was not related to the local wind.

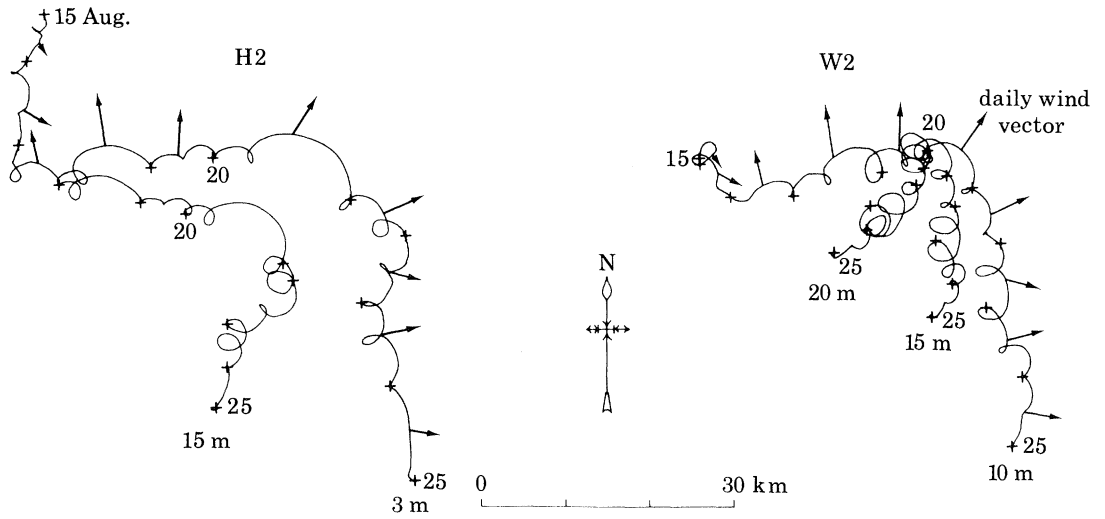

FIGURE 9. Progressive vector diagrams (left) of the surface flow at H2 (the flow at 60 m has been subtracted) and (right) at W2 (the flow at 85 m has been subtracted). The shallowest, 3 m at H2 and 10 m at W2, records are plotted from 15 to 25 August. Deeper records, 15 m at H2 and 15 and 20 m at W2, are plotted from 18 to 25 and 20 to 25 August, respectively. Daily averaged wind stress vectors are plotted with their tails at the noon position of each day of the shallowest progressive vector diagrams.

Because empirical orthogonal function 1 contained 93 % of the variability at 85 m on W2 and was nearly depth-independent, removing the deepest velocity record at W2 was similar to subtracting function 1 from the data. The residual left by subtracting function 1 is the sum of functions 2 and 3 plus a small amount (approximately 2–3 % of the total) of additional variability. Functions 2 and 3 are uncorrelated modes of variability and provide a description of the structure of the near-surface flow. Function 2 had a slab-like flow in the mixed layer, while function 3 had strong near-surface flow with flow in the opposite direction in a region below the base of the mixed layer. Temporal variability of function 2 was coherent with the local wind (figure 10) only at the inertial frequency. Temporal variability of function 3 was coherent with the local wind stress over a broad range of low frequencies. The inertial response in the mixed layer to wind forcing is typically slab-like. In JASIN the inertial response was slab-like, but different at H2 from that at W2 (Weller 1982). The nearly circular inertial motions were energetic but resulted in no net transport. Transport related to the local wind was associated with the low frequency wind-related flow described by function 3. Time series of function 3 evaluated at the depths of the current meters on W2 were low-pass filtered and used to estimate the wind-driven transport between the surface and 20 m and between 20 and 70 m. The near-surface transport was parallel to, but only approximately one third the size of the predicted Ekman transport; and the transport between 20 and 70 m was of the same magnitude but in the opposite direction to the predicted wind-driven transport (figure 11). In addition, functions 1 and 2 both had peaks in coherence with the wind at approximately 0.015–0.020 and 0.090 c/h, indicating that at these frequencies components of the velocity data existed that over a broad range of depths were

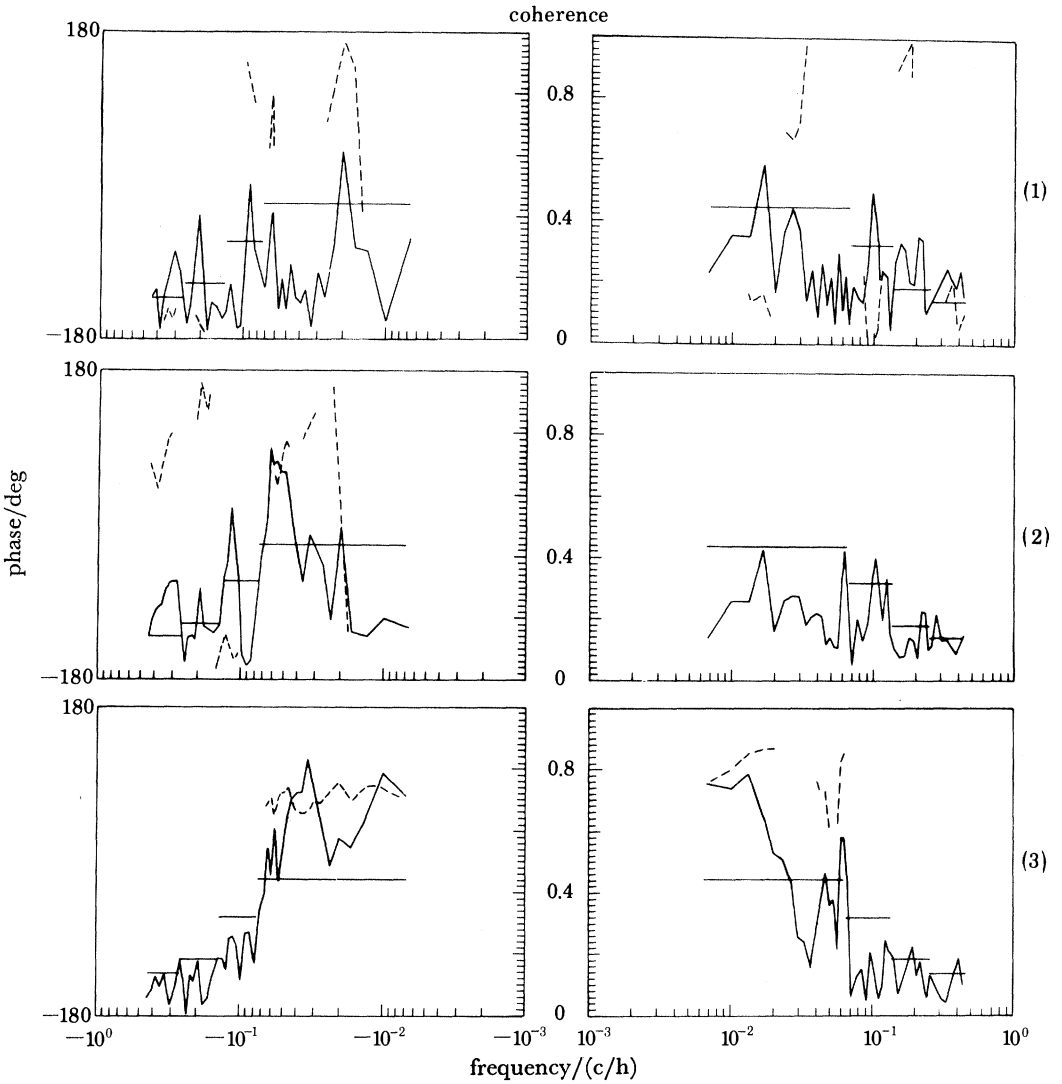

FIGURE 10. Coherence (solid lines) and phase (dashed lines) between the local wind stress and empirical orthogonal functions 1, 2, and 3 evaluated at 10 m on W2. The horizontal lines show the 95% confidence levels. The confidence levels vary with frequency owing to band-averaging that varied with frequency. Phase is shown only when the coherence exceeds the confidence level.

coherent with the local wind. These components, with approximately 2 cm s^{-1} mean amplitudes, were not, however, strong in comparison with the flow associated with the eddy.

5. Discussion

During JASIN 1978 much (*ca.* 87 % averaged over time and depth) of the velocity variability in the upper 310 m was due to tidal flow and to energetic eddies that drifted through the area of the experiment. In a region that extended from approximately 50 m below the mean depth of the base of the mixed layer down to 310 m the structure of the horizontal velocity field could be well described by one function or vertical pattern of horizontal velocity vectors. In the region in and just below the mixed layer significant velocity variability was associated with the two additional vertical patterns. The first of these had large-amplitude, depth-independent flow restricted to

PHILOSOPHICAL TRANSACTIONS OF THE ROYAL SOCIETY A MATHEMATICAL, PHYSICAL & ENGINEERING SCIENCES

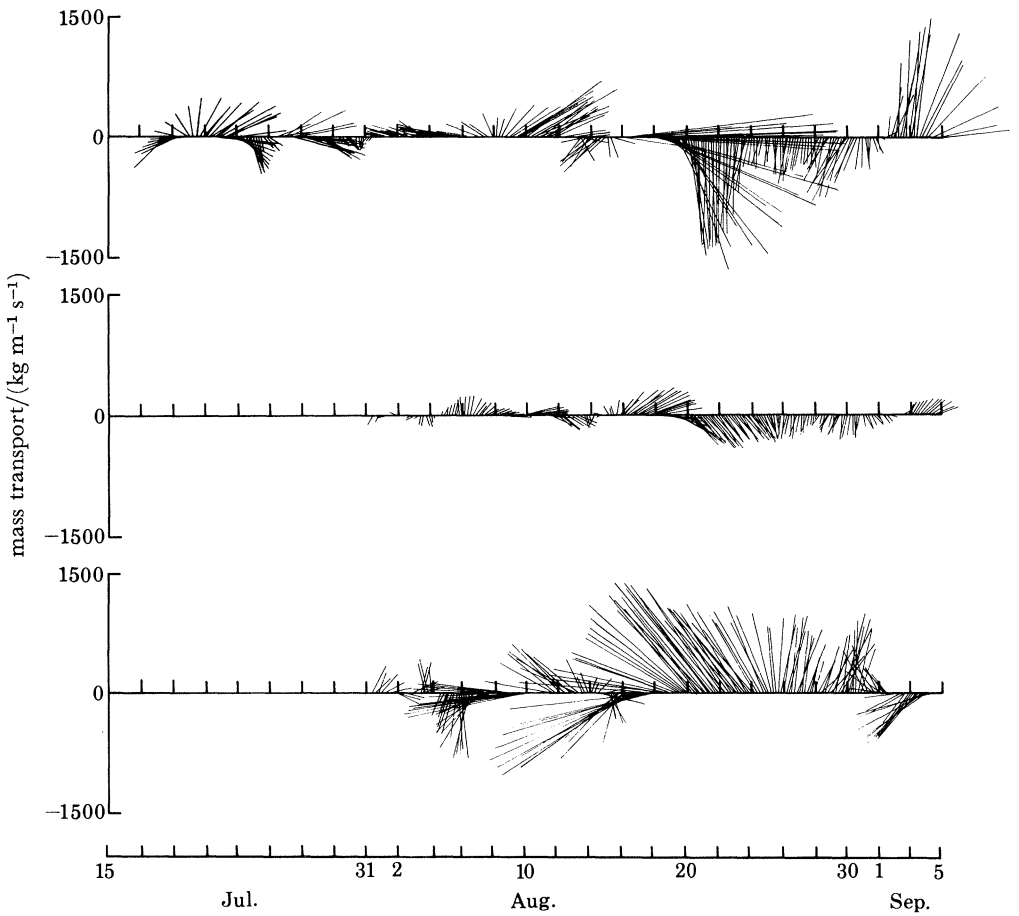

FIGURE 11. Comparison of the predicted Ekman mass transport (top) with the mass transport observed between the surface and 20 m (middle) and between 20 and 70 m (bottom) that was coherent with the wind. The near-surface transport is parallel to that predicted, but the deep transport is in the opposite direction.

within the mixed layer and only weak flow, in the opposite direction, found at greater depth. The second had strong flow near the surface that decayed with veering as a function of depth down to a minimum at the base of the mixed layer, and then increased in the opposite direction to a second maximum approximately 10 m below the mixed-layer base from which it again quickly decayed. In the near-surface region 65 % of the velocity variability was associated with the depth-independent flow (function 1). Of the remaining 35 %, some 20 % of the variability came from slab-like inertial oscillations and some 5 % from low frequency fluctuations, both of which were linearly related to the local wind. A significant fraction, 10 %, of the low frequency variability found in the mixed layer was neither related to the local wind nor related to deeper flow at that location.

When the wind was strong the near-surface flow at H2 resembled that at W2. The low frequency wind-related flow, but not the inertial motion, was a common component at both mooring locations. To some extent this flow was Ekman-like. It was to the right of the wind stress and veered with depth, but the angles between the flow and the wind were not those predicted by theory. Also, wind-related flow to the left of the wind stress was found below the base of the mixed layer. However, when the wind was not strong, the near-surface flow at W2 differed from

that at H2. In addition to the low frequency wind-related flow, which was common to both sites, there was low frequency flow near the surface that was not wind-related and was different at H2 from that at W2. Horizontal variability of the near-surface currents was, as a result, not wind-related.

At W2 the net displacement of fluid in the mixed layer associated with the low frequency non-wind-related, near-surface flow was 70 km to the southeast (from 30 July to 6 September). In contrast, the wind-related flow at 10 m resulted in a displacement of 40 km to the eastsoutheast. Advection of properties near the surface could not be modelled by adding to the quasi-geostrophic flow an Ekman velocity predicted from the observed wind stress. The additional non-wind-related flow found near the surface could not easily be modelled. The effect of that flow may, however, be distinguishable from the wind-related flow. The wind-driven component had vertical shear and would act to distort the distribution of properties in the mixed layer. The non-wind-related component was slab-like in the mixed layer and small in magnitude below; that flow will carry property distributions along in the mixed layer without distortion.

This paper has described several interesting characteristics of the flow observed during JASIN 1978:

(i) surface flow to the right of the wind, but only one third the size of the Ekman transport predicted from the local wind;

(ii) flow beneath the base of the mixed layer to the left of the wind;

(iii) flow variability at 0.09 and 0.02 c/h that at depths well below the mixed layer was related to the local wind;

(iv) flow near the surface that could be efficiently represented by only three empirical eigenfunctions.

The explanation for these characteristics and further study of the dynamics of the velocity field in the upper 300 m await the integration of these results with those presented in the other papers of this symposium.

The deployment of the VMCMs on W2 and initial data analysis of VMCM data was funded by the Office of Naval Research, contract N00014-74-C-0152 to Russ Davis at the Scripps Institution of Oceanography. Deployment of the W moorings and their instrumentation was funded by the Office of Naval Research, contract N00014-76-C-0197, NR 083-400 to Mel Briscoe at the Woods Hole Oceanographic Institution. Use of the VMCM and the W1 data is gratefully acknowledged. This work was funded by the Office of Naval Research, contract N00014-76-C-0197, NR 083-400 to the Woods Hole Oceanographic Institution (R.A.W.). The work benefited greatly from discussions with other JASIN participants and from the encouragement of R. T. Pollard. Nancy Pennington's assistance in preparation of the figures is gratefully acknowledged, as is Karin Bohr's assistance in preparation of the typescript. This is Woods Hole Oceanographic Institution contribution number 4990.

References

Davis, R. E. 1976 Predictability of sea surface temperature and sea level pressure anomalies over the North Pacific Ocean. *J. phys. Oceanogr.* **6**, 249–266.

Halpern, D., Weller, R. A., Briscoe, M. G., Davis, R. E. & McCullough, J. R. 1981 Intercomparison tests of moored current measurements in the upper ocean. *J. geophys. Res.* **86**, 419–428.

Large, W. G. & Pond, S. 1982 Sensible and latent heat flux measurements over the ocean. *J. phys. Oceanogr.* **12**, 464–482.

Payne, R. E. 1974 A buoy-mounted meteorological recording package. Woods Hole Oceanographic Institution Tech. Rep. no. WHOI 74-40 (32 pp.).

Pollard, R. T. 1982 Mesoscale (50–100 km) circulation revealed by inverse and classical analysis of the JASIN hydrographic data. *J. phys. Oceanogr.* (In the press.)

van Aken, H. M. & Prangsma, G. J. 1981 Fronts and meanders in the LSA. JASIN news, no. 23.

Weller, R. A. & Davis, R. E. 1980 A vector measuring current meter. *Deep-Sea Res.* **27**A, 565–581.

Weller, R. A., Payne, R., Briscoe, M. G. & Zenk, W. 1980 Preliminary report on surface wind from some of the JASIN oceanographic buoys. JASIN news, no. 21.

Weller, R. A. 1982 The relation of near-inertial motions observed in the mixed-layer during the JASIN (1978) experiment to the local wind stress and to the quasigeostrophic flow field. *J. phys. Oceanogr.* **12,** 1122–1136.

PHILOSOPHICAL TRANSACTIONS OF THE ROYAL SOCIETY A MATHEMATICAL, PHYSICAL & ENGINEERING SCIENCES